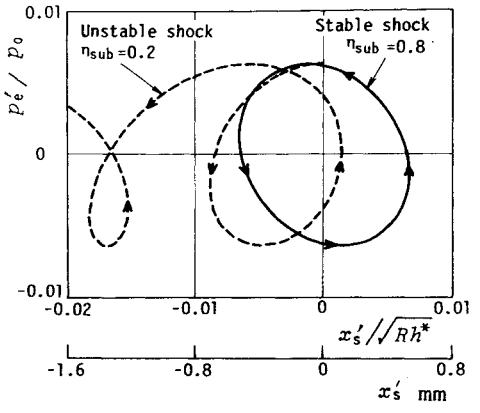

Fig. 2 Trajectories of shock wave in circular arc diffuser: $R=654$ mm, $h^*=10$ mm, $x_s/\sqrt{Rh^*}=0.2$, $M_1=1.23$, $\epsilon=0.01$, $f=500$ Hz.

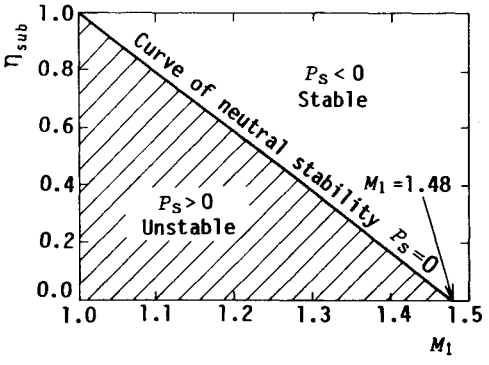

Fig. 3 Curve of neutral stability ($\gamma=1.4$).

the vertical axis represents p_e' divided by the stagnation pressure p_0 upstream of the diffuser; the arrows correspond to increasing time. In the case of $\eta_{sub}=0.8$, the trajectory shows a stable oscillation, whereas in the case of $\eta_{sub}=0.2$, the shock becomes unstable and is propagated upstream. Hence the behavior of the shock wave depends considerably on the diffuser efficiency for the subsonic flow downstream of the shock wave. It is evident from Eq. (1) that for $\tau>0$, the exponential term in Eq. (1) tends to zero and the shock oscillates stably, whereas if $\tau<0$, then x_s' approaches negative infinity, which implies the upstream propagation of the shock wave. For a divergent channel, the signs of τ and P_s are opposite [Eq. (2)]; accordingly, $P_s\leqq 0$ represents a criterion of the stability of the shock wave.

The relation between M_1 and α when $P_s=0$ is obtained from Eq. (8), eliminating α from the relation by the use of Eq. (11), yields the relation between η_{sub} and M_1. A calculated example is shown in Fig. 3. The shaded area where $P_s>0$ represents the unstable region. Figure 3 shows that the lower the Mach number M_1, i.e., the nearer the shock wave approaches the throat in the diffuser, the higher the diffuser efficiency is required for stability. The point of intersection of the curve of neutral stability and the horizontal axis gives $M_1=1.48$, which is the Mach number at which curve 4 in Fig. 1 becomes maximum. If a shock wave appears downstream of this point, the shock wave is always stable, regardless of the diffuser efficiency.

Conclusions

The behavior of a shock wave in a diffuser in response to small-amplitude pressure disturbances has been analyzed. The results suggest as follows:

1) The stability of the shock wave depends not only on the Mach number just upstream of the shock but also on the diffuser efficiency for subsonic flow downstream of the shock wave.

2) The curve of neutral stability that relates the diffuser efficiency η_{sub} to the Mach number M_1 is obtained. For gases with $\gamma=1.4$, the shock wave is always stable regardless of η_{sub} if $M_1>1.48$. For $1<M_1<1.48$, the maximum diffuser efficiency causing instability decreases as M_1 increases.

References

[1]Meier, G.E.A., "Shock Induced Flow Oscillations in a Laval Nozzle," *Symposium Transsonicum II*, edited by K. Oswatitsch and D. Rues, Springer-Verlag, Berlin, 1976, pp. 252–261.

[2]Chen, C. P., Sajben, M., and Kroutil, J. C., "Shock-Wave Oscillations in a Transonic Diffuser Flow," *AIAA Journal*, Vol. 17, Oct. 1979, pp. 1076–1083.

[3]Culick, F.E.C. and Rogers, T., "The Response of Normal Shocks in Diffusers," *AIAA Journal*, Vol. 21, Oct. 1983, pp. 1382–1390.

[4]Sajben, M., "The Response of Normal Shocks in Diffusers," *AIAA Journal*, Vol. 23, March 1985, pp. 477–478.

[5]Wegener, P. P. and Cagliostro, D. J., "Periodic Nozzle Flow with Heat Addition," *Combustion Science and Technology*, Vol. 23, 1973, pp. 269–277.

Unsteady Compressible Laminar Boundary-Layer Formed within a Centered Expansion Wave

T. J. Wang*
Chung-Shan Institute of Science and Technology
Lung-Tan, Taiwan

Introduction

THE purpose of this research is to investigate the effects of viscosity and heat transfer on the unsteady, compressible laminar boundary layer formed within a centered expansion wave traveling into a fluid at rest.[1,2] The temperature is at T_0 initially in the undisturbed high-pressure region. A centered expansion wave is formed at $t=0$ when the diaphram is burst and propagates into the undisturbed region. The qualitative expansion wave boundary layer is shown in Fig. 1. There have been numerous studies of the expansion wave problem.[1,2] It appears that the solutions given via a coordinate expansion of a series expansion method are restricted to the early stage of flow development. These results are less accurate for stations further downstream or later in time since the accuracy depends on the scale of the step size.

The present Note provides accurate and extensive solutions for a centered expansion wave advancing into quiescent fluid using the method of semisimilar solutions. The skin-friction distribution and heat-transfer distribution on the wall as determined by the present analysis are proven accurate by comparison with previous studies. The present study also presents results that are applicable at larger distances or at later times in the development of a centered expansion wave.

Received Dec. 3, 1986; revision received March 9, 1987.

*Research Assistant. Member AIAA.

Formulation and Solution

The differential equations governing the two-dimensional, unsteady, compressible flow under the Prandtl boundary-layer assumptions transform into nondimensional equations through the method of semisimilar solutions by the reduction of the number of variables from three to two. The two new variables are ξ and η separately.[3] The transformed governing equations and the boundary conditions employed here are identical to those of Ref. 3 and will not be repeated here. In the present problem, the similarity parameters are

$$\xi = 1 + x^*/t^*$$

and

$$\eta = \frac{1}{\sqrt{\nu_0 g(x,t)}} \int_0^y \frac{\rho}{\rho_0} dy$$

It is assumed that $u^* = u^*(\xi)$ and $g^{*2} = \xi t^*$ by carefully examining the inviscid flow functions. Here, the subscript δ designates the condition of the outer edge of the boundary layer in the expansion fan. The position of $\xi = 0$ is located at the expansion wavefront, and $\xi = 1$ is defined as the origin of the wave. The reference state is chosen at the expansion wavefront. The reference velocity U_r is related to the undisturbed region by the following relation:

$$U_r = \sqrt{\gamma R T_0}$$

The velocity temperature, pressure, and total enthalpy functions listed in the Appendix are the inviscid flow relations in an expansion wave. All of these relations are functions of ξ only. From these relations, the coefficients in the transformed governing equations become

$$a = 1 - \xi, \quad b = 1, \quad c = \xi(1 - \xi)$$

$$d = 2\xi/(\gamma + 1), \quad e = \xi/(\gamma + 1), \quad h = 2\xi^2/(\gamma + 1)$$

$$\ell = \frac{4}{(3\gamma - 1)} \left(\frac{\gamma - 1}{\gamma + 1} \right) \frac{\xi - 1}{H_\delta^*}$$

$$m = \left(\frac{\gamma - 1}{3\gamma - 1} \right) \left(\frac{2}{\gamma + 1} \xi \right)^2 \Big/ H_\delta^*$$

$$n = -\frac{4\gamma}{(3\gamma - 1)} \left(\frac{\gamma - 1}{\gamma + 1} \right) \left(1 - \frac{\gamma - 1}{\gamma + 1} \xi \right)^{[(\gamma+1)/(\gamma-1)]} \frac{T_\delta^*}{P_\delta^* H_\delta^*}$$

The two thermal wall boundary conditions correspond either to 1) the isothermal wall, or 2) the adiabatic wall.

In the isothermal wall case, the wall temperature is assumed to be T_0 (the initial temperature) at all times. The wall boundary condition in this case is given by

$$\theta_w(\xi) = H_w/H_\xi = 2/[(3\gamma - 1)H_\delta^*]$$

For the adiabatic wall case, the computer program has been written to meet the necessary boundary conditions. Thus, all of the coefficients are well defined as one proceeds to convert the transformed govering equations into a set of quasilinearized finite-difference equations.[4] The solutions for the transformed governing equations subject to the boundary conditions are obtained by the use of a modified implicit finite-difference technique.[4] The solution at each axial station is obtained iteratively and the iteration procedure is rather standard.[4]

In order to obtain a solution that satisfies the adiabatic wall conditions, it is necessary to add an additional iteration cycle to the problem. In this iteration process, the wall enthalpy is varied until that corresponding to zero heat transfer is obtained. For this additional iteration, new estimates of the wall enthalpy corresponding to zero heat transfer are obtained by the root-seeking method. With this condition, the specification of the problem is completed. The solution of the transformed governing equations subject to the boundary conditions may proceed as in the case for the isothermal wall condition.

Results and Conclusion

Solutions have been obtained for the case in which $Pr = 0.72$ and $\gamma = 1.4$. The total number of points across the boundary layer was set equal to 120 points.

Skin friction for the adiabatic wall and the isothermal wall boundary condition is plotted in Fig. 2. There are no significant differences between the present results and those of Refs. 1 and 2 for $\xi \leq 0.5$, but large differences would exist between them if the series expansion method were to be continued beyond $\xi = 0.5$. Skin friction for the isothermal wall condition is approximately 8.37% higher than that for the adiabatic wall condition at the trailing edge of the centered expansion wave.

The heat transfer from the wall to the fluid for the isothermal wall case is shown in Fig. 3. There is a difference of approximately 1.53% between the present analysis and previous studies at $\xi = 0.5$. The heat transfer increases rapidly behind the wavefront of the expansion fan and reaches its maximum value at $\xi = 0.38$. It then decreases further downstream. The precipitious increase of the kinetic energy, the boundary-layer thickness, and the skin friction behind the wavefront is the reason for the growth of the heat transfer rate until it reaches the peak value. Although the kinetic energy is increasing as ξ increases, the internal energy is decreasing so that the total enthalpy decreases with ξ. This result and the gradually decreasing thickness of the boundary layer reduce the heat-transfer rate along the wall, and it even overpasses the increasing effort of the skin friction in the heat transfer. Therefore, the heat-transfer rate decreases after reaching the peak value with increasing distance from the expansion wavefront.

The solution for the unsteady, laminar boundary-layer equations by the use of the semisimilar method exhibited a fairly good agreement between the present analysis and previous studies for $\xi < 0.5$. The method presented here also shows that the marching procedure of the finite-difference numerical technique can be carried as far as $\xi = 1.0$ for both wall boundary conditions. All of the results obtained in-

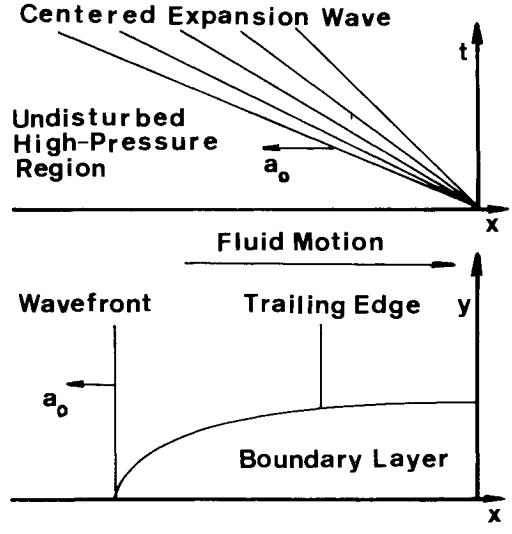

Fig. 1 Qualitative expansion wave boundary layer.

dicate that the numerical solutions are more accurate and can be carried farther than either the series expansion solutions or the coordinate expansion solutions.

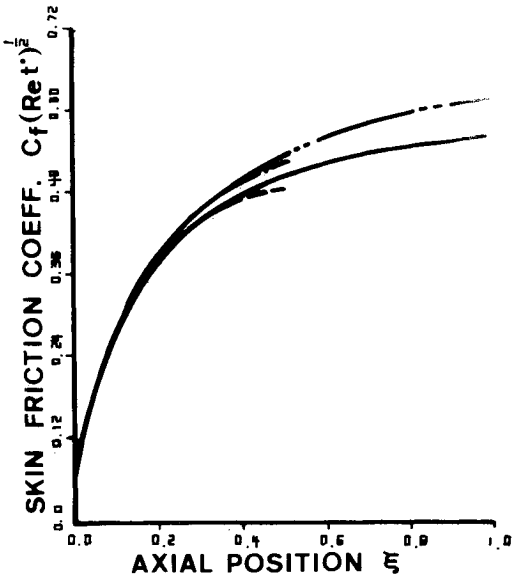

Fig. 2 Skin-friction distribution. Isothermal wall: – – –, present solution; – – –, Ref. 3. Adiabatic wall: –, present solution; – – –, Ref. 3.

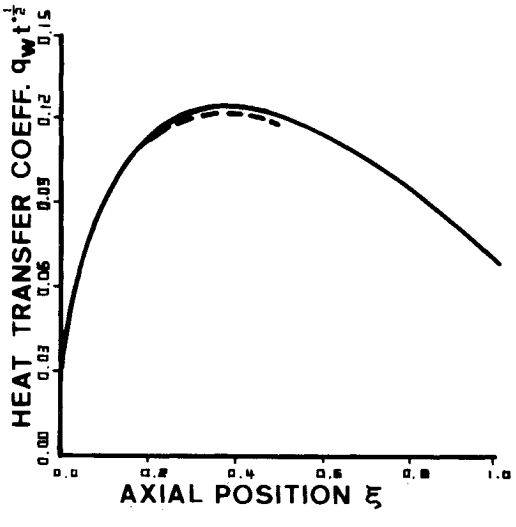

Fig. 3 Heat-transfer distribution for an isothermal wall: –, present solution; – – –, Ref. 3.

Appendix: Inviscid Flow Relation in a Centered Expansion Wave

Velocity:

$$u_\delta^* = \frac{2\xi}{\gamma+1}$$

Temperature:

$$T_\sigma^* = \left(1\frac{\gamma-1}{\gamma+1}\xi\right)^2\Big/\gamma$$

Pressure:

$$P_\delta^* = \left(1-\frac{\gamma-1}{\gamma+1}\xi\right)^{[2\gamma/(\gamma-1)]}$$

Total enthalpy:

$$H_\delta^* = \frac{2}{(3\gamma-1)}\left[\left(1-\frac{\gamma-1}{\gamma+1}\xi\right)^2+\left(\frac{2\xi}{\gamma+1}\right)\left(\frac{\gamma-1}{\gamma+1}\xi\right)\right]$$

References

[1]Hall, J. G., "Laminar Boundary Layers Developed within Unsteady Expansion and Compression Wave," *AIAA Journal,* Vol. 10, April 1972, pp. 499-505.

[2]Chang, L. M. and Chen, C-J., "Unsteady Compressible Laminar Boundary-Layer Flow within a Moving Expansion Wave," *AIAA Journal,* Vol. 19, Dec. 1981, pp. 1551-1557.

[3]Williams, J. C. III and Wang, T. J., "Semi-Similar Solutions of the Unsteady Compressible Laminar Boundary-Layer Equation," *AIAA Journal,* Vol. 23, Feb. 1985, pp. 228-233.

[4]Blottner, F. G., "Finite Difference of Solution of Boundary-Layer Equation," *AIAA Journal,* Vol. 8, Feb. 1970, pp. 193-205.

Extension of Hypersonic, High-Incidence, Slender-Body Similarity

Richard W. Barnwell*
NASA Langley Research Center, Hampton, Virginia

Introduction

An analysis of inviscid, hypersonic flow past slender bodies at large angles of attack developed by Sychev,[1] shows that these flows are governed by two parameters: the crossflow components of the Mach number and a parameter that relates thickness ratio and angle of attack. The analysis is discussed in well-known texts on hypersonic flow by Hayes and Probstein[2] and Cox and Crabtree.[3]

Recently, Hemsch[4] has shown that the Sychev parameters can be used to correlate experimental normal-force and pitching-moment data for a variety of configurations for Mach numbers from low supersonic to hypersonic. On purpose of this Note is to show that the Sychev analysis is applicable to all slender-body flows with crossflow Mach numbers greater than sonic and hence is not restricted to flows with hypersonic values of the cross flow Mach number as indicated in Refs. 1-3. Also, it will be shown that the Sychev similarity applies to a number of slender-body flows with subsonic crossflow Mach numbers, including incompressible flow.

Near-Field Analysis

The basic Sychev equations governing the inviscid flow in the near field or slender bodies at large angles of attack can be obtained with no assumption regarding Mach number. As shown in Fig. 1, a body-oriented Cartesian coordinate system is used with x in the axial direction and the freestream velocity vector in the x-y plane; the velocity components are u, v, and w. The body thickness and length parameters are d and l, respectively, such that the body thickness ratio δ satisfies the inequality

$$\delta = d/l \ll 1$$

Received Dec. 24, 1986; revision received March 19, 1987.

*Chief Scientist. Associate Fellow AIAA.